arXiv:1401.1595v3 [hep-ph] 21 Mar 2014

Higher bottom and bottom-strange mesons

Yuan Sun[1,2], Qin-Tao Song[1,3,6], Dian-Yong Chen[1,3], Xiang Liu[1,2*,†] and Shi-Lin Zhu[4,5‡§]

[1]*Research Center for Hadron and CSR Physics, Lanzhou University & Institute of Modern Physics of CAS, Lanzhou 730000, China*
[2]*School of Physical Science and Technology, Lanzhou University, Lanzhou 730000, China*
[3]*Nuclear Theory Group, Institute of Modern Physics of CAS, Lanzhou 730000, China*
[4]*Department of Physics and State Key Laboratory of Nuclear Physics and Technology, Peking University, Beijing 100871, China*
[5]*Collaborative Innovation Center of Quantum Matter, Beijing 100871, China*
[6]*University of Chinese Academy of Sciences, Beijing 100049, China*

Motivated by the recent observation of the orbital excitation $B(5970)$ by the CDF Collaboration, we have performed a systematic study of the mass spectrum and strong decay patterns of the higher B and B_s mesons. Hopefully the present investigation may provide valuable clues to further experimental exploration of these intriguing excited heavy mesons.

PACS numbers: 14.40.Nd, 12.38.Lg, 13.25.Hw

I. INTRODUCTION

The past decade has witnessed the discovery of many charmed and charmed-strange states such as $D_{sJ}(2317)$ [1–3], $D_s(2460)$ [2, 3], $D_{sJ}(2632)$ [4], $D_{sJ}(2860)$ [5], $D_{sJ}(2715)$ [6], $D_{sJ}(3040)$ [7], $D(2550)$ [8]/$D_J(2580)$ [9], $D^*(2600)$ [8]/$D_J^*(2650)$ [9], $D(2750)$ [8]/$D_J(2740)$ [9], $D^*(2760)$ [8]/$D_J^*(2760)$ [9], and $D_J^{(*)}(3000)$ [9], which have not only enriched the family of the charmed and charmed-strange states, but also stimulated extensive discussions of their properties (see Ref. [10] for a mini review of the research status of these newly observed charmed and charmed-strange states).

The present situation of the experimental exploration of bottom and bottom-strange states is strikingly similar to that of charmed and charmed-strange states in 2003; i.e., some candidates for the P-wave bottom and bottom-strange meson were announced [11–19] while the radially excited states seem whitin reach [20]. Very recently, the CDF Collaboration studied the orbitally excited B mesons, and reported that the new $B(5790)$ state could be the radially excited state in the bottom meson family [20]. There are several theoretical studies of the bottom and bottom-strange mesons before [21, 22] and after [23, 24] the experimental observation of these states.

Now is a good time to carry out a comprehensive theoretical study on higher bottom and bottom-strange mesons. In this work, we will calculate the mass spectrum of higher bottom and bottom-strange mesons and the corresponding two-body strong decay behavior. We hope the present investigation may not only shed light on the properties of the observed bottom and bottom-strange states, but also provide valuable clues to further experimental exploration of the radially and orbitally excited bottom and bottom-strange states.

This paper is organized as follows. After the Introduction, we present the analysis of the mass spectrum of the bottom and bottom-strange meson family in comparison with the available experimental data and other theoretical results. In Sec. III, we discuss the two-body strong decay behavior of the higher bottom and bottom-strange mesons. The last section is devoted to the discussion and Conclusion.

II. THE MASS SPECTRUM

We first calculate the mass spectrum of the higher bottom and bottom-strange mesons in the framework of the relativistic quark model [25], where the total Hamiltonian $\tilde{H}_1$ describes the interaction between quark and anti-quark in the meson

$$\tilde{H}_1 = \left(p^2 + m_1^2\right)^{1/2} + \left(p^2 + m_2^2\right)^{1/2} + \tilde{H}_{12}^{\rm conf} + \tilde{H}_{12}^{\rm so} + \tilde{H}_{12}^{\rm hyp}, \quad (1)$$

where $\tilde{H}_{12}^{\rm conf}$ denotes the confinement term and $\tilde{H}_{12}^{\rm so}$ is the spin-orbit term which can be decomposed into the symmetric part $\tilde{H}_{(12)}^{\rm so}$ and the antisymmetric part $\tilde{H}_{[12]}^{\rm so}$. In addition, $\tilde{H}_{12}^{\rm hyp}$ is the sum of the tensor and contact terms, i.e.,

$$\tilde{H}_{12}^{hyp} = \tilde{H}_{12}^{\rm tensor} + \tilde{H}_{12}^{\rm c}. \quad (2)$$

The concrete forms of these terms can be found in Appendix A of Ref. [25].

In the bases $|n^{2S+1}L_J\rangle$, the antisymmetric part of the spin-orbit term $\tilde{H}_{[12]}^{\rm so}$ and the tensor term $\tilde{H}_{12}^{\rm tensor}$ have nonvanishing off-diagonal elements, which result in the mixing of the states with quantum numbers ^3L_J and ^1L_J or with ^3L_J and $^3(L\pm2)_J$. Thus, the total Hamiltonian $\tilde{H}_1$ can be divided into two parts in this bases, which include the diagonal part $H_{\rm diag}$ and off-diagonal part $H_{\rm off}$ with the form

$$H_{\rm off} = \tilde{H}_{[12]}^{\rm so} + \left(\tilde{H}_{12}^{\rm tensor}\right)_{\rm off}, \quad (3)$$

where $\left(\tilde{H}_{12}^{\rm tensor}\right)_{\rm off}$ denotes the off-diagonal parts of $\tilde{H}_{12}^{\rm tensor}$. In the following, we first diagonalize $H_{\rm diag}$ in the simple harmonic oscillator bases and obtain the eigenvalues and eigenvectors corresponding to the wave function of the meson. One also needs to diagonalize the off-diagonal part $H_{\rm off}$ in the bases $|n^{2S+1}L_J\rangle$, which is treated as the perturbative term. We neglect the perturbative term $H_{\rm off}$ in the present calculation.

*Corresponding author
‡Corresponding author
†Electronic address: xiangliu@lzu.edu.cn
§Electronic address: zhusl@pku.edu.cn

The free parameters of the adopted relativistic quark model are listed in Table II of Ref. [25], which include the quark masses and the coefficients in the effective potential. Here, we list the quark masses

$$m_u = m_d = 220\,\text{MeV},\ m_b = 4977\,\text{MeV},\ m_s = 419\,\text{MeV}, \quad (4)$$

which are also applied in the following two-body strong decay calculation.

With the above preparation, we obtain the mass spectra of the bottom and bottom-strange meson families as shown in Fig. I, where the masses of the $1S$, $2S$, $3S$, $1P$, $2P$, $1D$, $2D$, and $1F$ states are given. Godfrey *et al.* calculated the mass spectrum of some of the bottom and bottom-strange mesons long ago [25]. We also notice that there exist predictions of the mass spectra of the bottom and bottom-strange mesons using other theoretical models. For example, Ebert *et al.* adopted the relativistic quark model based on the quasipotential approach [26] while the authors of Ref. [27] used the relativistic quark model with the Dirac Hamiltonian potential, where the correction of $1/m_b$ in the potential is also included. In addition, in Refs. [28, 29] the masses of the radial excitations of $D/D_s/B/B_s$ were predicted, which are comparable with the corresponding results listed in Table I.

In Fig. 1 and Table I, we list our results of the mass spectra of the bottom and bottom-strange meson families, the results from other groups, and compare them with the experimental data.

Until now, there has been only some limited experimental information on the low-lying bottom and bottom-strange mesons, which are shown in the fifth and ninth columns. The theoretical results can reproduce these experimental data well. When comparing our results with those given by Refs. [26, 27], we notice that the discrepancy of the values of the mass from different models is about 50 MeV for the $2S$, $3S$, and $1D$ states, while the mass difference for the $1F$, $2P$ and $2D$ states from different model calculations may reach up to about 100 $\sim$ 200 MeV. Thus, we will consider the mass dependence of the strong decay width of the higher bottom and bottom-strange mesons, which will be discussed in the next section. In the following, we will employ our numerical results to study the two-body strong decay behavior of these higher bottom and bottom-strange mesons.

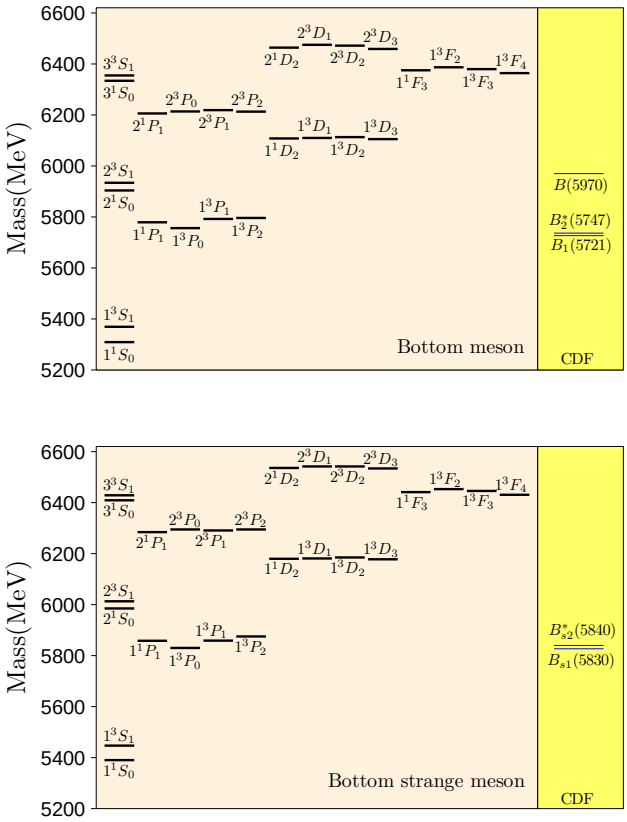

FIG. 1: (color online). The comparison of the mass spectrum of bottom and bottom-strange meson calculated by the relativistic quark model (see Table I for the concrete values) with the experimental data [11–20].

III. TWO-BODY STRONG DECAY BEHAVIOR

In this work, we will study the two-body strong decay of the higher bottom and bottom-strange mesons allowed by the Okubo-Zweig-Iizuka (OZI) rule, where the quark pair creation (QPC) model is adopted in our calculation.

The QPC model [31–37] is an effective approach to study the strong decay of hadrons, which has been widely applied to study the decay behaviors of the newly observed hadron states [38–45]. In the QPC model, the meson OZI-allowed decay occurs via the creation of a quark-antiquark pair from the vacuum. The created quark-antiquark pair is a flavor and color singlet with the vacuum quantum number $J^{PC} = 0^{++}$. The transition operator T is written as [46]

$$T = -3\gamma \sum_m \langle 1m; 1\ -m|00\rangle \int d\mathbf{k}_3 d\mathbf{k}_4 \delta^3(\mathbf{k}_3+\mathbf{k}_4) \times \mathcal{Y}_{1m}\left(\frac{\mathbf{k}_3-\mathbf{k}_4}{2}\right)\chi^{34}_{1,-m}\phi^{34}_0\omega^{34}_0 d^\dagger_{3i}(\mathbf{k}_3)b^\dagger_{4j}(\mathbf{k}_4), \quad (5)$$

where the flavor and color wave functions have the forms $\phi^{34}_0 = (u\bar{u} + d\bar{d} + s\bar{s})/\sqrt{3}$ and $\omega^{34}_0 = \delta_{ij}/\sqrt{3}$, respectively. The color indices are denoted by i and j. The solid harmonic polynomial is $\mathcal{Y}_{lm}(\mathbf{k}) = |\mathbf{k}|^l Y_{lm}(\mathbf{k})$. The spin wave function is $\chi^{34}_{1,-m}$ with an angular momentum quantum number $(1,-m)$. γ denotes the model parameter, which describes the strength of the quark-antiquark pair creation from the vacuum. In our calculation, the γ value is chosen to be 6.3 and $6.3/\sqrt{3}$ for the creations of u/d quark and s quark [41], respectively.

The helicity amplitude $\mathcal{M}^{M_{J_A}M_{J_B}M_{J_C}}(\mathbf{K})$ of the $A \to B + C$ decay is defined as

$$\langle BC|T|A\rangle = \delta^3(\mathbf{K}_B + \mathbf{K}_C - \mathbf{K}_A)\mathcal{M}^{M_{J_A}M_{J_B}M_{J_C}}(\mathbf{K}), \quad (6)$$

which can be further expressed as the product of the flavor, spin and spatial matrix elements, where the calculation of the

TABLE I: The obtained masses of the bottom and bottom-strange mesons in this work in comparison with the experimental values [30] and other theoretical results [26, 27]. In the second and sixth columns, the values listed in the brackets are the β values in the simple harmonic oscillator (SHO) wave function, which will be adopted in studying the strong decays of these higher bottom and bottom-strange mesons. Here, the β value in the SHO wave function is obtained by reproducing the realistic root-mean-square (rms) radius given by this work. In addition, we want to emphasize that the results from Refs. [26, 27] consider the mixing of the states with the same J^P quantum number.

$n^{2S+1}L_J$	Bottom meson				Bottom-strange meson			
	This work	Ref. [26]	Ref. [27]	Expt. [30]	This work	Ref. [26]	Ref. [27]	Expt. [30]
1^1S_0	5309(0.63)	5280	5279	5279.55 ± 0.26	5390(0.69)	5372	5373	5366.7 ± 0.4
1^3S_1	5369(0.57)	5326	5324	5325.2 ± 0.4	5447(0.63)	5414	5421	5415.8 ± 1.5
2^1S_0	5904(0.51)	5890	5886	–	5985(0.54)	5976	5985	–
2^3S_1	5934(0.50)	5906	5920	–	6013(0.53)	5992	6019	–
3^1S_0	6334(0.47)	6379	6320	–	6409(0.49)	6467	6421	–
3^3S_1	6355(0.46)	6387	6347	–	6429(0.48)	6475	6449	–
1^3P_2	5796(0.49)	5741	5714	5743 ± 5	5875(0.52)	5842	5820	5839.96 ± 0.20
1^3P_0	5756(0.56)	5749	5706	–	5830(0.59)	5833	5804	–
1^3P_1	5782(0.53)	5723	5700	5723.5 ± 2.0	5859(0.56)	5831	5805	5828.7 ± 0.4
1^1P_1	5779(0.52)	5774	5742	–	5858(0.55)	5865	5842	–
2^3P_2	6213(0.46)	6260	6188	–	6295(0.49)	6359	6292	–
2^3P_0	6214(0.49)	6221	6163	–	6279(0.51)	6318	6292	–
2^3P_1	6219(0.48)	6281	6175	–	6291(0.50)	6345	6278	–
2^1P_1	6206(0.48)	6209	6194	–	6284(0.50)	6321	6296	–
1^3D_3	6105(0.46)	6091	5933	–	6178(0.48)	6191	6103	–
1^3D_1	6110(0.50)	6119	6025	–	6181(0.52)	6209	6127	–
1^3D_2	6113(0.48)	6121	5985	–	6185(0.50)	6218	6095	–
1^1D_2	6108(0.48)	6103	6025	–	6180(0.50)	6189	6140	–
2^3D_3	6459(0.44)	6542	–	–	6534(0.46)	6637	–	–
2^3D_1	6475(0.47)	6534	–	–	6542(0.48)	6629	–	–
2^3D_2	6472(0.46)	6554	–	–	6542(0.47)	6651	–	–
2^1D_2	6464(0.46)	6528	–	–	6536(0.47)	6625	–	–
1^3F_4	6364(0.44)	6380	6226	–	6431(0.45)	6475	6337	–
1^3F_2	6387(0.47)	6412	6264	–	6453(0.48)	6501	6369	–
1^3F_3	6380(0.45)	6420	6220	–	6446(0.47)	6515	6332	–
1^1F_3	6375(0.45)	6391	6271	–	6441(0.47)	6468	6376	–

spatial matrix element is the most crucial part in the whole QPC calculation (see [46] for more details). In order to obtain the spatial matrix element, we adopt the mock state to describe the mesons [47]. In our calculation, the spatial radial wave function of the meson is represented by a SHO wave function [46] with a parameter β. The β values in the SHO wave functions are determined by reproducing the rms radius of the corresponding states calculated in the relativistic quark model. In Table I, we list these adopted β values for the bottom and bottom-strange mesons discussed.

Converting the helicity amplitude $\mathcal{M}^{M_{J_A}M_{J_B}M_{J_C}}(\mathbf{K})$ to the partial wave amplitude $\mathcal{M}_{SL}(|\mathbf{K}|)$ through the Jacob-Wick formula [48], we get

$$\mathcal{M}_{LS}(\mathbf{K}) = \frac{\sqrt{2L+1}}{2J_A+1}\sum_{M_{J_B},M_{J_C}}\langle L0S\,M_{J_A}|J_AM_{J_A}\rangle \times\langle J_BM_{J_B}J_CM_{J_C}|S\,M_{J_A}\rangle\mathcal{M}^{M_{J_A}M_{J_B}M_{J_C}}(\mathbf{K}). \quad (7)$$

Finally, the decay width relevant to the partial wave amplitude is

$$\Gamma = \pi^2\frac{|\mathbf{K}|}{M_A^2}\sum_{LS}|\mathcal{M}_{LS}(\mathbf{K})|^2\,, \quad (8)$$

where M_A is the mass of the initial meson A. We take the experimental mass as input if the corresponding decay involves the observed state. Otherwise, we take the predicted mass from the relativistic quark mode in Table I when studying the strong decay of the bottom and bottom-strange mesons.

In the following subsections, we illustrate the OZI-allowed strong decay behaviors of the bottom and bottom-strange mesons in detail. We use B and B_s to represent bottom and bottom-strange mesons, respectively.

A. Bottom meson

1. 1P and 2P states

TABLE II: The calculated partial and total decay widths (in units of MeV) of $2P$ states in the B meson family. The forbidden decay channels are marked by –. For the $2P(1^+)/2P'(1^+)$ states, we use □ to mark the allowed decay channels.

Channels	2^3P_0	2^3P_2	$2P(1^+)/2P'(1^+)$
πB	47	9.7×10^{-2}	–
πB^*	–	1.4	□
$\pi B(1^3P_0)$	–	–	□
$\pi B(1^3P_2)$	–	4.6	□
$\pi B(1P)$	10	16	□
$\pi B(1P')$	51	1.3	□
ηB	5.6	0.11	–
ηB^*	–	0.45	□
ρB	–	4.3	□
ρB^*	27	26	□
ωB	–	1.3	□
ωB^*	8.8	9.3	□
KB_s	3.6	1.3×10^{-2}	–
KB_s^*	–	0.11	□
K^*B_s	–	2.7×10^{-2}	–
Total	154	64	–

Although the predicted mass of the 1^3P_0 bottom meson is above both $B\pi$ and $B^*\pi$ thresholds, $B(1^3P_0)$ can only decay into $B\pi$. Its $B^*\pi$ decay is forbidden due to the parity conservation. The partial decay width of $B(1^3P_0)\to B\pi$ can reach up to 225 MeV. This state is very broad, which provides a natural explanation of why $B(1^3P_0)$ is still missing experimentally. There were other theoretical calculations of the decay width of the $B(1^3P_0)$ state. For example, the authors used the chiral quark model and obtained $\Gamma(B(1^3P_0)\to B\pi)=272$ MeV [23], which is consistent with our result.

The two $J^P=1^+$ states are the mixture of the 1^1P_1 and 1^3P_1 states

$$\begin{pmatrix} 1P(1^+)\\ 1P'(1^+)\end{pmatrix}=\begin{pmatrix}\cos\theta_{1P} & \sin\theta_{1P}\\ -\sin\theta_{1P} & \cos\theta_{1P}\end{pmatrix}\begin{pmatrix}1^1P_1\\ 1^3P_1\end{pmatrix}, \quad (9)$$

where θ_{1P} denotes the mixing angle. In general, in the heavy quark limit one has $\theta_{1P}=-54.7°$[49]. However, the obtained θ_{1P} value deviates from this ideal value when the heavy quark mass is finite in the case of the bottom and bottom-strange mesons. We will discuss this issue later.

In heavy quark effective theory, the heavy-light meson system can be categorized into different doublets by the angular momentum of the light component j_ℓ, which is a good quantum number in the limit of $m_Q\to\infty$. There are two 1^+ states in the $(0^+,1^+)$ and $(1^+,2^+)$ P-wave doublets, which correspond to $j_\ell=1/2^+$ and $j_\ell=3/2^+$, respectively. We can easily distinguish these two 1^+ states; i.e., the 1^+ state in the $(0^+,1^+)$ doublet is broad while the other 1^+ state in the $(1^+,2^+)$ doublet is narrow. In Eq. (9), the $1P(1^+)$ and $1P'(1^+)$ states correspond the 1^+ states in the $(0^+,1^+)$ and $(1^+,2^+)$ doublets, respectively. The following quantitative study of the decay behaviors will confirm the above qualitative observation.

In 2007, D0 Collaboration reported the observation of $B_1(5721)^0$ in the $B^{*+}\pi^-$ channel, where its measured mass is $5720.6\pm2.4\pm1.4$ MeV [15]. Later, CDF confirmed $B_1(5721)^0$ with the mass $5725.3^{+1.6+1.4}_{-2.2-1.5}$ MeV [16]. Very recently, CDF [20] studied the orbitally excited B mesons by using the full CDF Run II data sample. Besides confirming $B_1(5721)$, CDF reported the width of $B_1(5721)$ for the first time, where the measured width is $20\pm2\pm5$ MeV and $42\pm11\pm13$ MeV for the neutral and charged $B_1(5721)$ states [20], respectively. Since $B_1(5721)$ has a narrow width, $B_1(5721)$ is a good candidate of the $1P'(1^+)$ state in the B meson family.

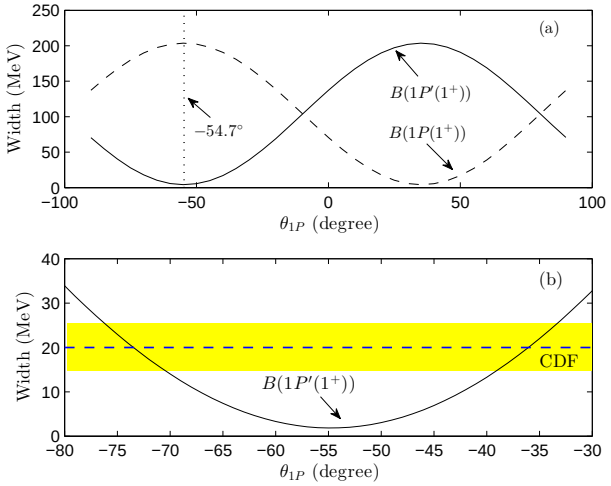

FIG. 2: (color online). (a) The dependence of the total decay widths of $B(1P(1^+))$ (dashed curve) and $B(1P'(1^+))$ (solid curve) on the mixing angle θ_{1P}. (b) The dependence of the total width of $B(1P'(1^+))$ on the mixing angle $\theta_{1P}=(-80\sim-30)°$ and the comparison with the CDF data [20]. Here, the vertical dashed line in (a) corresponds to the ideal mixing angle $\theta_{1P}=-54.7°$.

For $B_1(5721)$, its dominant decay is $B^*\pi$. With the QPC model, we calculate $B_1(5721)^0\to B^*\pi$. In Fig. 2, the dependence of the calculated width of $B_1(5721)^0$ on the mixing angle θ_{1P} is given. If taking the ideal value $\theta_{1P}=-54.7°$, the corresponding width of $B_1(5721)^0$ is 1.8 MeV, which is far smaller than the experimental data. We find that the calculated width of $B_1(5721)^0$ overlaps with the experimental value when θ_{1P} is in the range of $(-77°\sim-70°)$ or $(-40°\sim-33°)$. We also predict the width of $B(1P(1^+))$ state, where is $\Gamma(B(1P(1^+)))=170\sim197$ MeV corresponding to $\theta_{1P}=(-77°\sim-70°)$ or $(-40°\sim-33°)$, which confirms $B(1P(1^+))$ is a broad state.

$B_2^*(5747)$ was first observed by D0 in its $B^{*+}\pi^-$ and $B^+\pi^-$ channels [15]. Other experimental information of $B_2^*(5747)^0$ given by D0 includes: $M(B_2^*(5747)^0)=5746.8\pm2.4\pm1.7$

MeV and $\Gamma(B_2^*(5747)^0 \to B^{*+}\pi^-)/\Gamma(B_2^*(5747)^0 \to B^{(*)+}\pi^-) = 0.475 \pm 0.095 \pm 0.069$ [15]. In 2009, CDF announced the confirmation of $B_2^*(5747)^0$ with mass $M = 5740.2^{+1.7+0.9}_{-1.8-0.8}$ MeV and width $\Gamma = 22.7^{+3.8+3.2}_{-3.2-10.2}$ MeV [16]. In Ref. [20], CDF again carried out the study of $B_2^*(5747)$. The mass and width are $M = 5736.6 \pm 1.2 \pm 1.2 \pm 0.2/5737.1 \pm 1.1 \pm 0.9 \pm 0.2$ MeV and $\Gamma = 26 \pm 3 \pm 3/17 \pm 6 \pm 8$ MeV, respectively for the neutral/charged $B_2^*(5747)$ states [20].

As a $J^P = 2^+$ B meson, $B_2^*(5747)$ decays into the $B\pi$ and $B^*\pi$ channels. In the QPC model, the total decay width of $B_2^*(5747)^0$ is around 3.7 MeV, which is composed of $\Gamma(B_2^*(5747)^0 \to B\pi) = 1.9$ MeV and $\Gamma(B_2^*(5747)^0 \to B^*\pi) = 1.8$ MeV. We notice that our result of the total decay width of $B_2^*(5747)^0$ is smaller than the experimental central value [16, 20]. As shown in Refs. [16, 20], there exist large experimental errors for the measured width of $B_2^*(5747)$. Thus, further experimental measurement of the resonance parameter of $B_2^*(5747)$ will be helpful to clarify this difference. In addition, we also obtain the ratio

$$\frac{B(B_2^*(5747) \to B^{*+}\pi^-)}{B(B_2^*(5747) \to B^+\pi^-)} = 0.95, \qquad (10)$$

which is consistent with the experimental value $1.10 \pm 0.42 \pm 0.31$ [15].

For the $2P$ states in the B meson family, more decay channels are open. However, there has been no experimental observation up to now. We list our predictions of the partial and total decay widths in Table II.

For the $B(2^3P_0)$ meson, the dominant decay modes are $\pi B(1P')$, πB, and ρB^*. In addition, $B(2^3P_0)$ can decay into ωB^*, KB_s, ηB, and $\pi B(1P)$. The sum of all partial decay widths of $B(2^3P_0)$ reaches up to 154 MeV, which indicates $B(2^3P_0)$ is a broad state. Among the dominant decay channels of $B(2^3P_0)$, πB is the most suitable channel for searching $B(2^3P_0)$.

$B(2^3P_2)$ mainly decays into ρB^*, $\pi B(1P)$, ωB^*, and $\pi B(1^3P_2)$, where the partial width of $B(2^3P_2) \to \rho B^*$ is the largest since $B(2^3P_2) \to \rho B^*$ occurs via S-wave. In contrast, the D-wave decay modes $B(2^3P_2) \to \pi B$, KB_s, K^*B_s can be neglected. The width of $B(2^3P_2)$ is 64 MeV.

As the mixture of the 2^1P_1 and 2^3P_1 states, the two 1^+ states $B(2P(1^+))$ and $B(2P'(1^+))$ satisfy the following relation

$$\begin{pmatrix} 2P(1^+) \\ 2P'(1^+) \end{pmatrix} = \begin{pmatrix} \cos\theta_{2P} & \sin\theta_{2P} \\ -\sin\theta_{2P} & \cos\theta_{2P} \end{pmatrix} \begin{pmatrix} 2^1P_1 \\ 2^3P_1 \end{pmatrix}, \qquad (11)$$

where θ_{2P} denotes the mixing angle. The allowed decay modes of $B(2P(1^+))$ and $B(2P'(1^+))$ are shown in Table II.

We obtain the total and partial decay widths of $B(2P(1^+))$ and $B(2P'(1^+))$, which depend on the mixing angle θ_{2P} (see Fig. 3 for details). Since the experimental information of $B(2P(1^+))$ and $B(2P'(1^+))$ is absent, in the following discussion we take the typical value $\theta_{2P} = -54.7°$. We find that the total decay width of $B(2P(1^+))$ ($\Gamma(B(2P(1^+))) = 153$ MeV) is larger than that of $B(2P'(1^+))$ ($\Gamma(B(2P'(1^+))) = 70$ MeV), which is consistent with the estimate under the heavy quark effective theory. For $B(2P(1^+))$ and $B(2P'(1^+))$, its main decay channels include πB^*, $\pi B(1^3P_2)$, $\pi B(1P'(1^+))$, ρB^* and $\pi B(1P(1^+))$. In addition, the other decay modes of $B(2P(1^+))$ and $B(2P'(1^+))$ are also presented in Fig. 3.

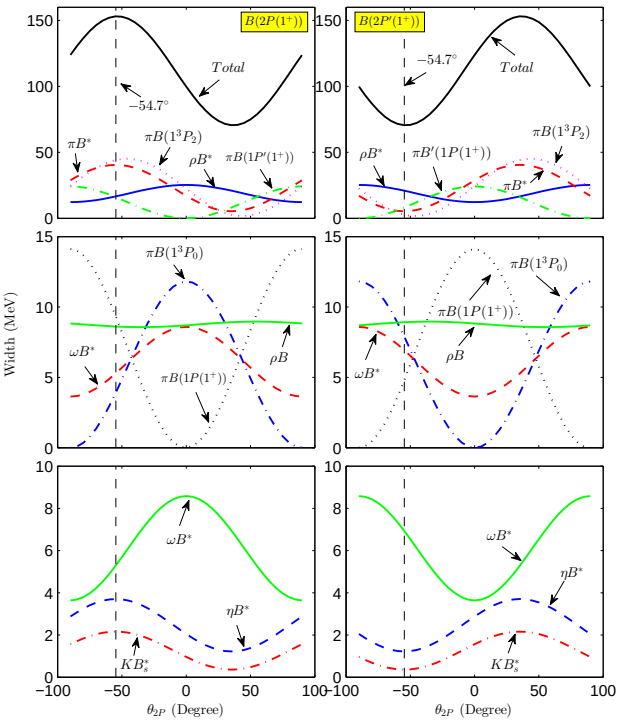

FIG. 3: (color online). The dependence of the decay behavior of $B(2P(1^+))$ (the first column) and $B(2P'(1^+))$ (the second column) on the mixing angle θ_{2P}.

2. 2S and 3S states

Very recently, the CDF Collaboration reported the evidence of a new resonance $B(5970)$ in analyzing both $B^0\pi^+$ and $B^+\pi^-$ mass distributions [20]. The mass and width of $B(5970)$ are

$$(M,\Gamma)_{B(5970)^0} = (5978 \pm 5 \pm 12,\ 70 \pm 18 \pm 31)\,\text{MeV},$$
$$(M,\Gamma)_{B(5970)^+} = (5961 \pm 5 \pm 12,\ 60 \pm 20 \pm 40)\,\text{MeV},$$

which correspond to the neutral and charged $B(5970)$, respectively. The comparison of the mass of $B(5970)$ and the mass spectrum in Table I indicates that the mass of $B(5970)$ is close to the estimated masses of the 2^1S_0 and 2^3S_1 states of the B meson family. Since $B(5970)$ can decay into $B\pi$, we can exclude the $B(2^1S_0)$ assignment of $B(5970)$.

The obtained total width of $B(2^3S_1)$ is 47 MeV, which is in agreement with the experimental width of $B(5970)$ if one considers the experimental error. The calculation of the partial decay widths of $B(2^3S_1)$ indicates that πB^*, πB and $\pi B(1P(1^+))$ are its main decay channels. The results of the other partial decay widths of $B(2^3S_1)$ are listed in Table III. At present, $B(5970)$ was only observed in the πB channel. Our study indicates that the $B(5970)$ is very probably $B(2^3S_1)$. We also

TABLE III: The partial and total decay widths (in units of MeV) of $2S$ and $3S$ states in the B meson family. Here, we adopt – to denote the forbidden decay channels.

Channels	2^1S_0	2^3S_1	3^1S_0	3^3S_1
πB	–	9.1	–	2.6
πB^*	33	23	8.8	6.1
$\pi B(1^3P_0)$	3.9	–	3.7	–
$\pi B(1^3P_2)$	2.0×10^{-3}	1.0×10^{-2}	11.2	4.9
$\pi B(1P(1^+))$	–	10	–	3.9
$\pi B(1P'(1^+))$	–	0.2	–	2.8
ηB	–	1.2	–	0.49
ηB^*	0.62	2.0	1.0	0.87
$\eta B(1^3P_0)$	–	–	0.16	–
$\eta B(1^3P_2)$	–	–	7.2×10^{-2}	8.8×10^{-2}
$\eta B(1P(1^+))$	–	–	–	0.28
$\eta B(1P'(1^+))$	–	–	–	0.11
ρB	–	–	1.3	1.3
ρB^*	–	–	9.4	7.0
ωB	–	–	0.49	5.7×10^{-2}
ωB^*	–	–	3.3	1.7
KB_s	–	0.43	–	0.24
KB_s^*	–	0.58	0.45	0.41
K^*B_s	–	–	0.46	0.27
$K^*B_s^*$	–	–	0.49	0.90
$KB_s(1^3P_0)$	–	–	4.0×10^{-2}	–
$KB_s(1^3P_2)$	–	–	–	2.8×10^{-3}
$KB_s(1P(1^+))$	–	–	–	0.10
$KB_s(1P'(1^+))$	–	–	–	3.7×10^{-3}
Total	38	47	41	33

suggest the experimental search for $B(5970)$ via its πB^* decay.

As the partner of $B(2^3S_1)$, $B(2^1S_0)$ dominantly decays into πB^*. In addition, there exists a considerable partial width of $B(2^1S_0)\to\pi B(1^3P_0)$. Compared with the πB^* and $\pi B(1^3P_0)$, the remaining two decay channels ηB^* and $\pi B(1^3P_2)$ can be ignored. Thus, πB^* is the ideal channel to search for $B(2^1S_0)$ in future experiments.

The masses of the two $3S$ states $B(3^1S_0)$ and $B(3^3S_1)$ are 6334 MeV and 6355 MeV, respectively. As shown in Table III, more decay channels are open for $B(3^1S_0)$ and $B(3^3S_1)$. The main decay modes of $B(3^1S_0)$ are $\pi B(1^3P_2)$, ρB^*, πB^*, ωB^*. For $B(3^3S_1)$, mainly ρB^*, πB^*, $\pi B(1^3P_2)$, $\pi B(1P(1^+))$, $\pi B(1P'(1^+))$, πB, ωB^*, and ρB contribute to the total decay width. The partial widths of the modes $\eta B(1^3P_2)$, ωB, $KB_s(1^3P_2)$ and $KB_s(1P'(1^+))$ are quite small.

TABLE IV: The partial and total decay widths (in units of MeV) of $1D$ and $2D$ states in the B meson family. The forbidden decay channels are marked by –. For the $1D(2^-)/1D'(2^-)$ and $2D(2^-)/2D'(2^-)$ states, we use □ to mark the allowed decay channels. Here, the value $a\times10^{-b}$ is abbreviated as $a[b]$.

Channels	1^3D_1	1^3D_3	2^3D_1	2^3D_3	$1D(2^-)$ $1D'(2^-)$	$2D(2^-)$ $2D'(2^-)$
πB	69	4.9	27	1.2	–	–
πB^*	34	6.2	12	0.49	□	□
$\pi B(1^3P_0)$	–	–	–	–	□	□
$\pi B(1^3P_2)$	1.6	0.74	5.3	0.21	□	□
$\pi B(1P(1^+))$	6.8[2]	9.0[2]	8.1	6.4	□	□
$\pi B(1P'(1^+))$	147	0.17	28	7.5[2]	□	□
ηB	12	0.21	4.3	5.8[2]	–	–
ηB^*	5.6	0.20	1.6	1.2[3]	□	□
$\eta B(1^3P_0)$	–	–	–	–	–	□
$\eta B(1^3P_2)$	–	–	0.62	0.19	–	□
$\eta B(1P(1^+))$	–	–	0.74	0.57	–	□
$\eta B(1P'(1^+))$	–	–	0.65	2.1[2]	–	□
ρB	8.3	1.8[2]	0.12	2.0	□	□
ρB^*	0.93	1.3	23	6.1	□	□
ωB	2.4	3.7[3]	3.2[2]	0.67	□	□
ωB^*	0.10	–	7.5	2.0	□	□
KB_s	7.4	5.4[2]	2.5	4.4[2]	–	–
KB_s^*	3.3	4.5[2]	0.86	8.6[3]	□	□
K^*B_s	–	–	0.25	1.9[3]	–	□
$K^*B_s^*$	–	–	0.65	0.75	–	□
$KB_s(1^3P_0)$	–	–	–	–	–	□
$KB_s(1^3P_2)$	–	–	0.20	4.5[2]	–	□
$KB_s(1P(1^+))$	–	–	0.19	0.12	–	□
$KB_s(1P'(1^+))$	–	–	0.14	4.2[3]	–	□
Total	294	14	122	23	–	–

3. $1D$ and $2D$ states

The decay behaviors of $1D$ and $2D$ states are given in Table IV, where we first list the allowed decay channels for the $1D(2^-)/1D'(2^-)$ $2D(2^-)/2D'(2^-)$ states.

$B(1^3D_1)$ is very broad and its total width reaches up to 294 MeV. $B(1^3D_1)$ dominantly decays into $\pi B(1P'(1^+))$, πB and πB^*. These channels are suitable to search for $B(1^3D_1)$ in future experiments. $B(2^3D_1)$ is the first radial excitation of $B(1^3D_1)$. We notice that $\pi B(1P'(1^+))$, πB, ρB^*, and πB^* are the main decay modes of $B(2^3D_1)$, which renders $B(2^3D_1)$ broad. Different from the broad $B(1^3D_1)$ and $B(2^3D_1)$, $B(1^3D_3)$ and $B(2^3D_3)$ are rather narrow states since the total decay widths of $B(1^3D_3)$ and $B(2^3D_3)$ are 14 and 23 MeV, respectively. For $B(1^3D_3)$, there exist two dominant decay channels, πB and πB^*. Although more decay modes are included for $B(2^3D_3)$, its total decay width is not obviously enhanced. The $\pi B(1P(1^+))$, ρB^*, ρB, ωB^* and πB are the main

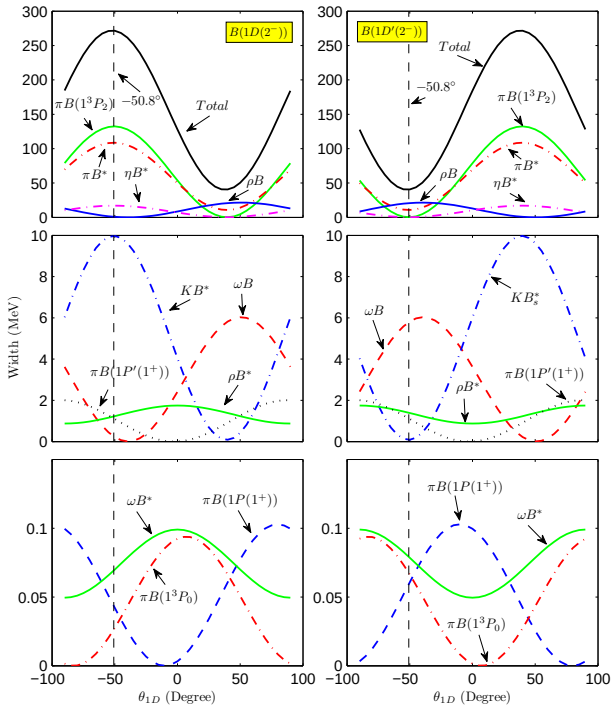

FIG. 4: (color online). The dependence of the decay behavior of $B(1D(2^-))$ (the first column) and $B(1D'(2^-))$ (the second column) on the mixing angle θ_{1D}.

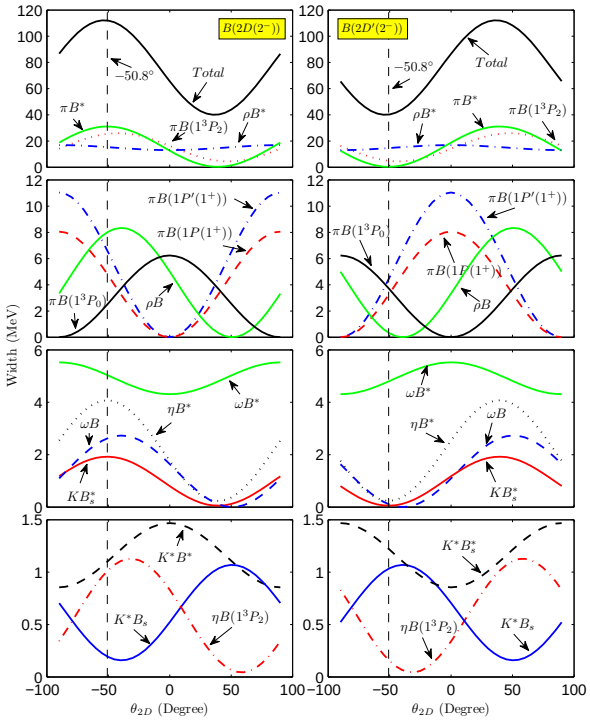

FIG. 5: (color online). The dependence of the partial and total decay widths of $B(2D(2^-))$ (the first column) and $B(2D'(2^-))$ (the second column) on the mixing angle θ_{2D}.

decay modes of $B(2^3D_3)$. The concrete information of the decay pattern of $B(1^3D_1)$, $B(2^3D_1)$, $B(1^3D_3)$ and $B(2^3D_3)$ can be found in Table IV.

$B(nD(2^-))$ and $B(nD'(2^-))$ are the mixture of the n^3D_2 and n^1D_2 states, which satisfy the following relation:

$$\begin{pmatrix} nD(2^-) \\ nD'(2^-) \end{pmatrix} = \begin{pmatrix} \cos\theta_{nD} & \sin\theta_{nD} \\ -\sin\theta_{nD} & \cos\theta_{nD} \end{pmatrix} \begin{pmatrix} n^1D_2 \\ n^3D_2 \end{pmatrix} \quad (12)$$

with $n = 1, 2$.

In Fig. 4, we present the dependence of the partial and total decay widths of $B(1D(2^-))$ and $B(1D'(2^-))$ on the mixing angle θ_{1D}. In the heavy quark limit, the mixing angle $\theta_{1D} = -50.8°$ was given in Ref. [49]. $\pi B(1^3P_2)$ and πB^* are the dominant decays for $B(1D(2^-))$ while ρB, πB^*, and ωB are the main contribution to the width of $B(1D'(2^-))$. The QPC calculation further indicates that the total width of $B(1D(2^-))$ is quite broad. Compared with the total decay width of $B(1D(2^-))$, the total decay width of $B(1D'(2^-))$ is narrow. Here, we need to specify that the above conclusion is obtained with the typical value $\theta_{1D} = -50.8°$. The decay behaviors of the partial decay widths of $B(2D(2^-))$ and $B(2D'(2^-))$ depend on the concrete value of θ_{1D} (see Fig. 4 for more details).

The variation of the total and partial decay widths of $B(2D(2^-))$ and $B(2D'(2^-))$ with θ_{2D} is shown in Fig. 5, from which we can obtain the main and subordinate decays of these two states. The total widths of $B(2D(2^-))$ and $B(2D'(2^-))$ are 112 and 40 MeV, respectively, corresponding to $\theta_{2D} = -50.8°$.

4. $1F$ states

There are four $1F$ states. Their decay pattern is listed in Table V. We notice that the total decay width of $B(1^3F_2)$ is quite broad, and can reach up to 254 MeV. Among all decays of $B(1^3F_2)$, $\pi B(1P'(1^+))$ is the most important channel. The other main decay modes of $B(1^3F_2)$ are πB, πB^*, $\pi B(1^3P_2)$, $\eta B(1P'(1^+))$, ρB, and ρB^*. For $B(1^3F_4)$, its total width is estimated as 103 MeV, where ρB^* and ωB^* are its dominant decay mode.

In the following, we focus on $B(1F(3^+))$ and $B(1F'(3^+))$, which are the mixing of the 1^3F_3 and 1^1F_3 states,

$$\begin{pmatrix} 1F(3^+) \\ 1F'(3^+) \end{pmatrix} = \begin{pmatrix} \cos\theta_{1F} & \sin\theta_{1F} \\ -\sin\theta_{1F} & \cos\theta_{1F} \end{pmatrix} \begin{pmatrix} 1^1F_3 \\ 1^3F_3 \end{pmatrix}. \quad (13)$$

with θ_{1F}=−49.1° determined in heavy quark limit [26]. In Fig. 6, the θ_{1F} dependence of the partial and total decay widths of $B(1F(3^+))$ and $B(1F'(3^+))$ is presented. If we take the typical value θ_{1F}=−49.1°, we notice that $B(1F(3^+))$ is a quite broad resonance. From Fig. 6, we can easily distinguish the main decay mode among all allowed decay channels, and we can distinguish which channel is valuable to further experimental search of the $1F$ state in the B meson family.

TABLE V: The partial and total decay widths (in units of MeV) of $1F$ states in B meson family. The forbidden decay channels are marked by –. For $1F(3^+)/1F'(3^+)$ states, we use □ to mark the allowed decay channels.

Channels	1^3F_2	1^3F_4	$1F(3^+)/1F'(3^+)$
πB	30	3.7	–
πB^*	21	5.3	□
$\pi B(1^3P_0)$	–	–	□
$\pi B(1^3P_2)$	14	2.5	□
$\pi B(1P(1^+))$	0.5	1.2	□
$\pi B(1P'(1^+))$	121	0.48	□
ηB	5.5	0.31	–
ηB^*	3.9	0.41	□
$\eta B(1^3P_0)$	–	–	□
$\eta B(1^3P_2)$	0.10	4.9×10^{-3}	–
$\eta B(1P(1^+))$	1.3×10^{-3}	7.4×10^{-3}	□
$\eta B(1P'(1^+))$	11	2.4×10^{-3}	□
ρB	15	1.1	□
ρB^*	15	56	□
ωB	4.7	0.33	□
ωB^*	2.2	31	□
KB_s	2.8	7.2×10^{-2}	–
KB_s^*	2.0	9.2×10^{-2}	□
K^*B_s	0.75	1.3×10^{-2}	□
$K^*B_s^*$	8.8×10^{-2}	0.24	–
$KB_s(1^3P_0)$	–	–	□
$KB_s(1^3P_2)$	1.1×10^{-3}	1.2×10^{-4}	–
$KB_s(1P(1^+))$	5.4×10^{-4}	2.0×10^{-4}	□
$KB_s(1P'(1^+))$	3.3	4.9×10^{-5}	□
Total	254	103	–

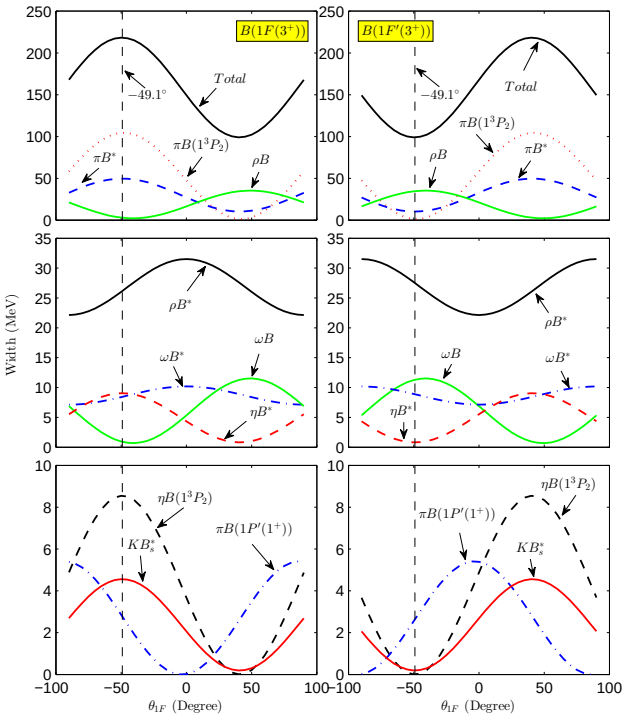

FIG. 6: (color online). The dependence of the partial and total decay widths of $B(1F(3^+))$ (the first column) and $B(1F'(3^+))$ (the second column) on the mixing angle θ_{1F}.

B. Bottom-strange meson

1. 1P and 2P states

The decay modes of $B_s(1^3P_0)$ is BK. The partial width of $B_s(1^3P_0) \to BK$ obtained from the QPC model is 225 MeV, which is almost the same as that from the chiral quark model in Ref. [23] (Γ = 227 MeV). $B_s(1^3P_0)$ is also a broad state, very similar to $B(1^3P_0)$. Generally speaking, it is difficult to detect a very broad state experimentally.

The observed $B_{s1}(5830)$ and $B_{s2}^*(5840)$ are good candidates of $B_s(1P'(1^+))$ and $B_s(1^3P_2)$, respectively. The experimental information on $B_{s1}(5830)$ and $B_{s2}^*(5840)$ from the CDF, D0, and LHCb Collaborations [17–20] is collected in Table VI.

If we take the mass of $B_{s2}^*(5840)$ as input, $B_s(1^3P_2)$ can decay into BK and B^*K. With the QPC model, the total decay width of $B_s(1^3P_2)$ is around $\Gamma(B_s(1^3P_2)) = 0.26$ MeV and slightly smaller than the experimental central value which has a large error [19, 20]. However, the obtained ratio

$$\frac{\Gamma(B_{s2}^* \to B^{*+}K^-)}{\Gamma(B_{s2}^* \to B^+K^-)} = 0.088 \qquad (14)$$

is in good agreement with the experimental measurement

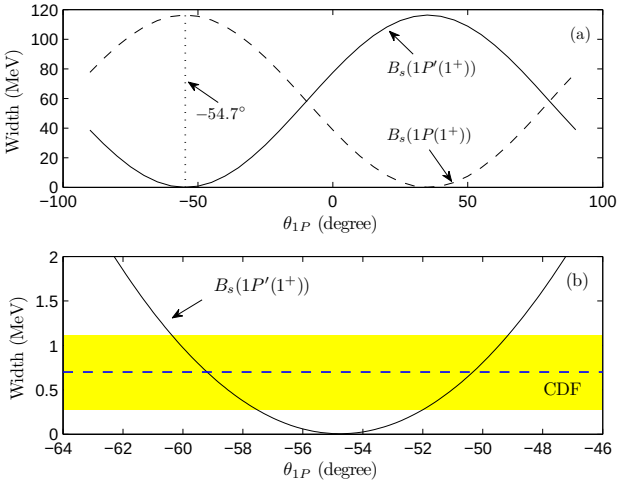

FIG. 7: (color online). (a) The dependence of the total decay widths of $B_s(1P(1^+))$ (dashed curve) and $B_s(1P'(1^+))$ (solid curve) on the mixing angle θ_{1P}. (b) The variation of the total width of $B_s(1P'(1^+))$ with the mixing angle $\theta_{1P} = (-64 \sim -46)^\circ$ and the comparison with the CDF data [20]. Here, the vertical dashed line in (a) corresponds to the ideal mixing angle $\theta_{1P} = -54.7^\circ$.

TABLE VI: The summary of experimental information of $B_{s1}(5830)$ and $B^*_{s2}(5840)$.

State	Collaboration	Mass	Width	Observed decays	$\frac{\Gamma(B^*_{s2}\to B^{*+}K^-)}{\Gamma(B^*_{s2}\to B^+K^-)}$
$B_{s1}(5830)$	CDF [17]	5829.4 ± 0.7 MeV	–	$B^{*+}K^-$	–
	LHCb [19]	$5828.40 \pm 0.04 \pm 0.04 \pm 0.41$	–	$B^{*+}K^-$	–
	CDF [20]	$5828.3 \pm 0.1 \pm 0.1 \pm 0.4$	$0.7 \pm 0.3 \pm 0.3$	$B^{*+}K^-$	–
$B^*_{s2}(5840)$	CDF [17]	5839.6 ± 0.7	–	B^+K^-	–
	D0 [18]	$5839.6 \pm 1.1 \pm 0.7$	–	B^+K^-	–
	LHCb [19]	$5839.99 \pm 0.05 \pm 0.11 \pm 0.17$	$1.56 \pm 0.13 \pm 0.47$	$B^{*+}K^-$, B^+K^-	$0.093 \pm 0.013 \pm 0.012$
	CDF [20]	$5839.7 \pm 0.1 \pm 0.1 \pm 0.2$	$2.0 \pm 0.4 \pm 0.2$	$B^{*+}K^-$, B^+K^-	0.11 ± 0.03

given by LHCb [19] and CDF [20], as shown in Table VI.

In analogy to $B(1P(1^+))$ and $B(1P'(1^+))$, $B_s(1P(1^+))$ and $B_s(1P'(1^+))$ are the mixture of the 1^3P_1 and 1^1P_1 states in the B_s meson family, which also satisfy Eq. (9). There only exists the B^*K decay channel for $B_s(1P(1^+))$ and $B_s(1P'(1^+))$. Thus, we give the dependence of the total decay widths of $B_s(1P(1^+))$ and $B_s(1P'(1^+))$ on the mixing angle θ_{1P} (see Fig. 7). When the mixing angle is taken as $\theta_{1P} = -60.5^\circ \sim -57.5^\circ$ or $-52.0^\circ \sim -49.0^\circ$, the total decay width of $B_s(1P'(1^+)$ overlaps the observed width of $B_{s1}(5830)$ given by CDF [20]. We notice that there exists a difference between the realistic and ideal value of the mixing angle θ_{1P}, which is similar to the situation of $B_1(5721)$. If adopting $\theta_{1P} = -60.5^\circ \sim -57.5^\circ$ or $-52.0^\circ \sim -49.0^\circ$, the total decay width of $B_s(1P(1^+)$ is about 110 MeV. Hence, $B_s(1P(1^+)$ is a broad resonance, consistent with the rough estimate in heavy quark limit.

TABLE VII: The partial and total decay widths (in units of MeV) of $2P$ states in the B_s meson family. The forbidden decay channels are marked by –. For $2P(1^+)/2P'(1^+)$ states, we use □ to mark the allowed decay channels.

Channels	2^3P_0	2^3P_2	$2P(1^+)/2P'(1^+)$
KB	65	2.6	–
KB^*	–	7.3	□
K^*B	–	1.6	□
K^*B^*	36	69	□
$KB(1^3P_0)$	–	–	□
$KB(1^3P_0)$	–	–	□
$KB(1P(1^+))$	5.3	0.70	□
$KB(1P'(1^+)$	32	3.5×10^{-3}	□
ηB_s	1.7	5.3×10^{-2}	–
ηB^*_s	–	0.14	□
Total	142	82	–

The decay behavior of the four $2P$ states are listed in Table VII, where $B_s(2P(1^+))$ and $B_s(2P'(1^+))$ are the mixed states satisfying Eq. (11). The three main decay channels for $B_s(2^3P_0)$ are KB, K^*B^*, and $KB(1P'(1^+))$. The sum of all partial decay widths listed in the second column of Fig.

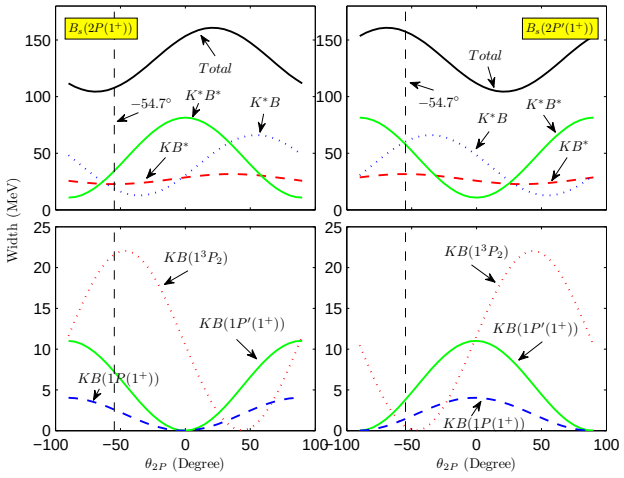

FIG. 8: (color online). The variation of the decay width of $B_s(1P(1^+))$ (the first column) and $B_s(1P'(1^+))$ (the second column) with the mixing angle θ_{2P}. Here, we only listed their main decay channels.

8 leads to the total decay width around 142 MeV. Thus, $B_s(2^2P_0)$ is a broad B_s meson. For $B_s(2^3P_2)$, there is only one dominant decay channel K^*B^*, where the branching ratio of $B_s(2^3P_2) \to K^*B^*$ is 0.84. At present, $B_s(2^3P_0)$ and $B_s(2^3P_2)$ are still missing. Thus, the obtained main decay modes of $B_s(2^3P_0)$ and $B_s(2^3P_2)$ may be useful to the experimental search of $B(2^3P_0)$ and $B(2^3P_2)$.

The dependence of the total and partial decay widths of $B_s(2P(1^+))$ and $B_s(2P'(1^+))$ on θ_{2P} are presented in Fig. 8. If θ_{2P} takes the typical value, the main decay modes are $B_s(2P(1^+))/B_s(2P'(1^+)) \to K^{(*)}B^{(*)}$ (see Fig. 8 for detailed information). We conclude that both $B_s(2P(1^+))$ and $B_s(2P'(1^+))$ are broad B_s states,

C. $2S$ and $3S$ states

In the following, we illustrate the decay behavior of $B_s(2^1S_0)$, $B_s(2^3S_1)$, $B_s(3^1S_0)$, and $B_s(3^3S_1)$ (see Table VIII).

TABLE VIII: The partial and total decay widths (in units of MeV) of $2S$ and $3S$ states in the B_s meson family. Here, we adopt – to denote the forbidden decay channels.

Channels	2^1S_0	2^3S_1	3^1S_0	3^3S_1
KB	–	17	–	5.8
KB^*	44	34	15	12
K^*B	–	–	3.0	0.41
K^*B^*	–	–	21	12
$KB(1^3P_0)$	–	–	9.8×10^{-4}	–
$KB(1^3P_2)$	–	–	14	7.5
$KB(1P(1^+))$	–	–	–	0.95
$KB(1P'(1^+))$	–	–	–	6.0
ηB_s	–	0.29	–	0.17
ηB_s^*	0.14	0.30	0.28	0.26
$\eta B_s(1^3P_0)$	–	–	0.11	–
$\eta B_s(1^3P_2)$	–	–	5.4×10^{-3}	1.2×10^{-2}
$\eta B_s(1P(1^+))$	–	–	–	0.15
$\eta B_s(1P'(1^+))$	–	–	–	1.3×10^{-2}
ϕB_s	–	–	0.26	0.31
Total	44	51	54	46

According to the numerical results in Table VIII, we conclude:

- $B_s(2^1S_0)$ dominantly decays into KB^*. The contribution from $\eta B_s(0^+)$ is negligible.
- KB^* and KB are the two main decays of $B_s(2^3S_1)$. The contribution from both ηB_s^* and $\eta B_s(0^+)$ decay modes is quite small.
- As the radial excitation of $B_s(2^1S_0)$, the total decay width of $B_s(3^1S_0)$ is $\Gamma(B_s(3^1S_0)) = 54$ MeV. Here, the branching ratios of $B_s(3^1S_0)) \to KB^*, K^*B^*, KB(1^3P_2)$ are 0.28, 0.39, and 0.26, respectively.
- The main decay modes of $B_s(3^3S_1))$ include KB^*, K^*B^*, KB, $KB(1^3P_2)$ and $KB(1P'(1^+))$.

D. $1D$ and $2D$ states

In Table IX, we list the numerical results of $B_s(1^3D_1)$, $B_s(1^3D_3)$, $B_s(2^3D_1)$ and $B_s(2^3D_3)$ and the allowed decay channels of $B_s(1D(2^-))/B_s(1D'(2^-))$ and $B_s(2D(2^-))/B_s(2D'(2^-))$.

Our calculation shows

- Both $B_s(1^3D_1)$ and its radial excitation $B_s(2^3D_1)$ are very broad, while both $B_s(1^3D_3)$ and $B_s(2^3D_3)$ are quite narrow.
- The dominant decay modes of $B_s(1^3D_1)$ are KB and KB^* with the branching ratios 0.65 and 0.30, respectively.

TABLE IX: The partial and total decay widths (in units of MeV) of $1D$ and $2D$ states in the B_s meson family. The forbidden decay channels are marked by –. For the $1D(2^-)/1D'(2^-)$ and $2D(2^-)/2D'(2^-)$ states, we use □ to mark the allowed decay channels. Here, the value $a\times10^{-b}$ is abbreviated as $a[b]$.

Channels	1^3D_1	1^3D_3	2^3D_1	2^3D_3	$1D(2^-)$ $1D'(2^-)$	$2D(2^-)$ $2D'(2^-)$
KB	125	5.2	49	0.61	–	–
KB^*	58	5.7	21	1.4[2]	□	□
K^*B	1.1	3.0[5]	0.99	5.5	□	□
K^*B^*	–	–	41	13	–	□
$KB(1^3P_0)$	–	–	–	–	–	□
$KB(1^3P_2)$	–	–	9.7	4.3	–	□
$KB(1P(1^+))$	–	–	12	11	–	□
$KB(1P'(1^+))$	–	–	33	0.38	–	□
ηB_s	4.8	5.3[2]	1.7	1.2[2]	–	–
ηB_s^*	2.0	4.5[2]	0.60	2.2[5]	□	□
$\eta B_s(1^3P_0)$	–	–	–	–	–	□
$\eta B_s(1^3P_2)$	–	–	0.16	5.8[2]	–	□
$\eta B_s(1P(1^+))$	–	–	0.16	0.14	–	□
$\eta B_s(1P'(1^+))$	–	–	0.13	6.3[3]	–	□
ϕB_s	–	–	0.38	6.7[2]	–	□
ϕB_s^*	–	–	0.70	1.7	–	□
Total	191	11	171	37	–	–

- $B_s(2^3D_1)$ mainly decays into KB, K^*B^*, $KB(1P'(1^+))$, KB^*, $KB(1P(1^+))$, and $KB(1^3P_2)$.
- For $B_s(1^3D_3)$, there are two dominant decay modes, KB and KB^*. For $B_s(2^3D_3)$, K^*B^*, $KB(1P(1^+))$, K^*B, and $KB(1^3P_2)$ are its main decay channels, while the remaining decay channels have small partial decay widths (see Table IX for more details).

As the mixed states $B_s(1D(2^-))/B_s(1D'(2^-))$ and $B_s(2D(2^-))/B_s(2D'(2^-))$ are similar to $B(1D(2^-))/B(1D'(2^-))$ and $B(2D(2^-))/B(2D'(2^-))$ in Eq. (12), in Figs. 9 and 10 we thus show the variation of their partial and total decay widths with θ_{1D}/θ_{2D}. With the typical $\theta_{1D} = \theta_{2D} = -50.8°$, we have the following observations:

- For $B_s(1D(2^-))/B_s(1D'(2^-))$, its KB^* mode is very important. The variation of the partial width $B_s(1D(2^-))/B_s(1D'(2^-)) \to KB^*$ with the mixing angle is very similar to that of the total decay width (see Fig. 9).
- $B_s(2D(2^-))$ is broad and mainly decays into KB^*, $KB(1^3P_2)$, K^*B^*, and K^*B. As the parter of $B_s(2D(2^-))$, the total decay width of $B_s(2D'(2^-))$ is smaller than that of $B_s(2D(2^-))$. The main decay mode of $B_s(2D'(2^-))$ is K^*B^*. While the sum of the partial decay widths of the decay modes $KB(1P(1^+)), KB(1^3P_0), KB(1P'(1^+)), K^*B$ is compara-

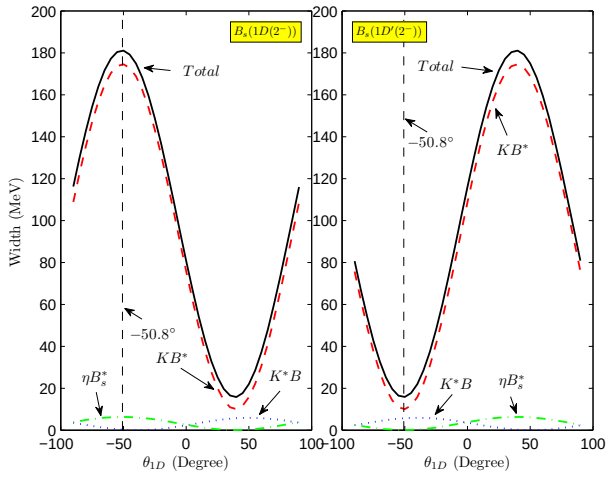

FIG. 9: (color online). The dependence of the decay behavior of $B_s(1D(2^-))$ (the first column) and $B_s(1D'(2^-))$ (the second column) on the mixing angle θ_{1D}.

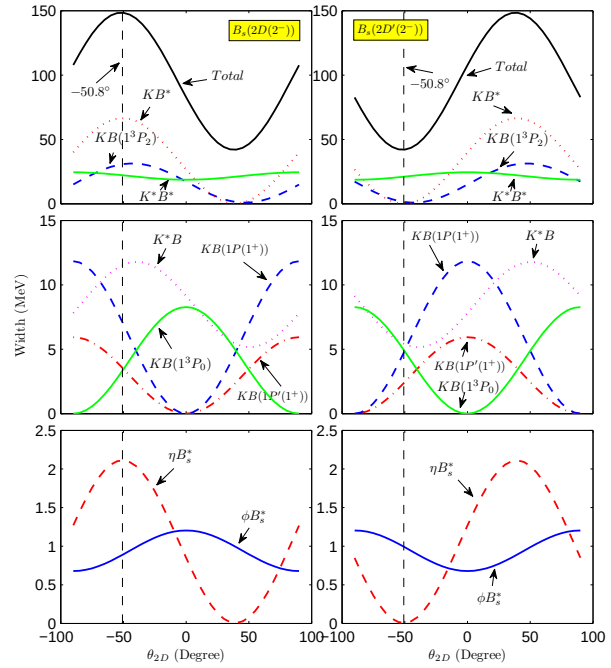

FIG. 10: (color online). The dependence of the partial and total decay widths of $B_s(2D(2^-))$ (the first column) and $B_s(2D'(2^-))$ (the second column) on the mixing angle θ_{2D}.

ble with the partial decay width of $B_s(2D'(2^-)) \to K^*B^*$.

E. $1F$ states

The decay behavior of the four $1F$ states is presented in Table X and Fig. 11.

- $B_s(1^3F_2)$ is a very broad resonance. Its total decay width can reach up to 319 MeV. The branching ratio of the $KB(1P'(1^+))$ mode is around 50%. The other important decay modes are $K^{(*)}B^{(*)}$ and $KB(1^3P_2)$.
- $B_s(1^3F_4) \to K^*B^*$ dominates the total decay width of $B_s(1^3F_4)$.
- The total and partial decay widths of $B_s(1F(3^+))$ and $B_s(1F'(3^+))$ are dependent on the mixing angle θ_{1F} in Eq. (13). In Fig. 11, the main and subordinate decay modes are given for $B_s(1F(3^+))$ and $B_s(1F'(3^+))$.

TABLE X: The partial and total decay widths (in units of MeV) of $1F$ states in the B_s meson family. The forbidden decay channels are marked by –. For $1F(3^+)/1F'(3^+)$ states, we use □ to mark the allowed decay channels.

Channels	1^3F_2	1^3F_4	$1F(3^+)$
KB	55	5.7	–
KB^*	38	7.4	□
K^*B	28	1.7	□
K^*B^*	26	100	□
$KB(1^3P_0)$	–	–	□
$KB(1^3P_2)$	17	0.94	□
$KB(1P(1^+))$	0.34	0.55	□
$KB(1P'(1^+))$	149	0.27	□
ηB_s	1.9	7.3×10^{-2}	–
ηB_s^*	1.4	8.9×10^{-2}	□
$\eta B_s(1^3P_0)$	–	–	□
$\eta B_s(1^3P_2)$	0.24	3.0×10^{-4}	□
$\eta B_s(1P(1^+))$	5.4×10^{-3}	3.8×10^{-4}	□
$\eta B_s(1P'(1^+))$	2.4	9.8×10^{-5}	□
ϕB_s	0.14	7.1×10^{-5}	□
ϕB_s^*	2.3×10^{-3}	–	□
Total	319	116	–

In the above discussions, we take the predicted mass values of these higher B and B_s meson families as input. However, the uncertainty of the calculated masses sometimes is around (50 ~ 200) MeV from various theoretical models. Therefore, when predicting the decay behavior of these higher B and B_s mesons, we also study the variations of their decay behavior with the mass of the parent state, which is illustrated in Fig. 12.

IV. SUMMARY

Inspired by the recent experimental observation of the orbital excitation $B(5970)$ for the first time by CDF Collaboration [20], we have carried out a systematic study of the higher B and B_s mesons. We have calculated both the masses of the higher B and B_s mesons and their OZI-allowed two-body strong decay patterns.

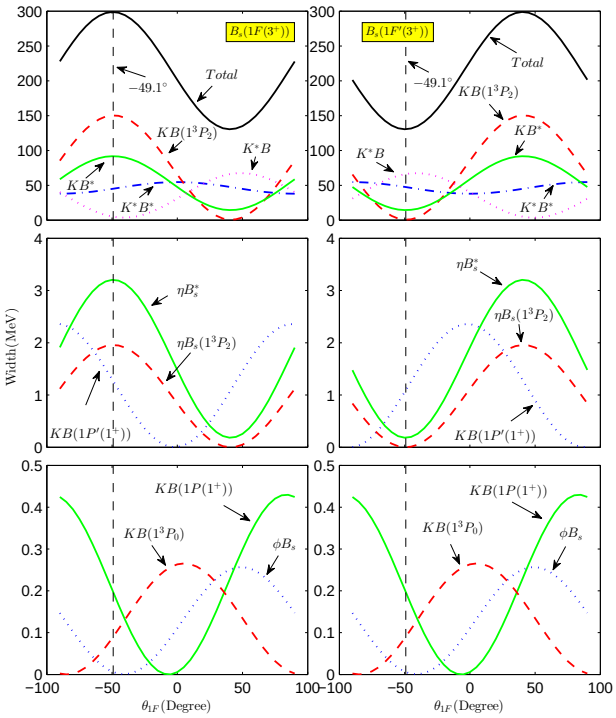

FIG. 11: (color online). The variation of the partial and total decay widths of $B_s(1F(3^+))$ (the first column) and $B_s(1F'(3^+))$ (the second column) with the mixing angle θ_{1F}.

At present, the status of studying B and B_s mesons is very similar to that of the D and D_s mesons in 2003. In the past several years, CDF, D0, and LHCb Collaborations have played a very important role in the study of the radial and orbital excitations of the B and B_s meson families. The higher radial and orbital excitations of the B and B_s mesons begin to emerge in experiment. In the coming years, LHCb has the potential to discover more and more excited B and B_s mesons. Hopefully our present investigation will be helpful to future experimental searchs for these interesting heavy mesons.

Acknowledgements

This project is supported by the National Natural Science Foundation of China under Grants No. 11222547, No. 11175073, No. 11035006, No. 11375240 and No. 11261130311, the Ministry of Education of China (FANEDD under Grant No. 200924, SRFDP under Grant No. 2012021111000, and NCET), and the Fok Ying Tung Education Foundation (Grant No. 131006).

[1] B. Aubert *et al.* [BaBar Collaboration], Phys. Rev. Lett. **90**, 242001 (2003) [hep-ex/0304021].
[2] D. Besson *et al.* [CLEO Collaboration], Phys. Rev. D **68**, 032002 (2003) [Erratum-ibid. D **75**, 119908 (2007)] [hep-ex/0305100].
[3] P. Krokovny *et al.* [Belle Collaboration], Phys. Rev. Lett. **91**, 262002 (2003) [hep-ex/0308019].
[4] A. V. Evdokimov *et al.* [SELEX Collaboration], Phys. Rev. Lett. **93**, 242001 (2004) [hep-ex/0406045].
[5] B. Aubert *et al.* [BaBar Collaboration], Phys. Rev. Lett. **97**, 222001 (2006) [hep-ex/0607082].
[6] K. Abe *et al.* [Belle Collaboration], hep-ex/0608031.
[7] B. Aubert *et al.* [BaBar Collaboration], Phys. Rev. D **80**, 092003 (2009) [arXiv:0908.0806 [hep-ex]].
[8] P. del Amo Sanchez *et al.* [BaBar Collaboration], Phys. Rev. D **82**, 111101 (2010) [arXiv:1009.2076 [hep-ex]].
[9] RAaij *et al.* [LHCb Collaboration], JHEP **1309**, 145 (2013) [arXiv:1307.4556 [hep-ex]].
[10] X. Liu, Int. J. Mod. Phys. Conf. Ser. **2**, 147 (2011).
[11] P. Abreu *et al.* [DELPHI Collaboration], Phys. Lett. B **345**, 598 (1995).
[12] R. Akers *et al.* [OPAL Collaboration], Z. Phys. C **66**, 19 (1995).
[13] D. Buskulic *et al.* [ALEPH Collaboration], Z. Phys. C **69**, 393 (1996).
[14] R. Barate *et al.* [ALEPH Collaboration], Phys. Lett. B **425**, 215 (1998).
[15] V. M. Abazov *et al.* [D0 Collaboration], Phys. Rev. Lett. **99**, 172001 (2007) [arXiv:0705.3229 [hep-ex]].
[16] T. Aaltonen *et al.* [CDF Collaboration], Phys. Rev. Lett. **102**, 102003 (2009) [arXiv:0809.5007 [hep-ex]].
[17] T. Aaltonen *et al.* [CDF Collaboration], Phys. Rev. Lett. **100**, 082001 (2008) [arXiv:0710.4199 [hep-ex]].
[18] V. M. Abazov *et al.* [D0 Collaboration], Phys. Rev. Lett. **100**, 082002 (2008) [arXiv:0711.0319 [hep-ex]].
[19] RAaij *et al.* [LHCb Collaboration], Phys. Rev. Lett. **110**, 151803 (2013) [arXiv:1211.5994 [hep-ex]].
[20] T. A. Aaltonen *et al.* [CDF Collaboration], arXiv:1309.5961 [hep-ex].
[21] A. F. Falk and T. Mehen, Phys. Rev. D **53**, 231 (1996) [hep-ph/9507311].
[22] A. H. Orsland and H. Hogaasen, Eur. Phys. J. C **9**, 503 (1999) [hep-ph/9812347].
[23] X. -H. Zhong and Q. Zhao, Phys. Rev. D **78**, 014029 (2008) [arXiv:0803.2102 [hep-ph]].
[24] Z. -G. Luo, X. -L. Chen and X. Liu, Phys. Rev. D **79**, 074020 (2009) [arXiv:0901.0505 [hep-ph]].
[25] S. Godfrey and N. Isgur, Phys. Rev. D **32**, 189 (1985).
[26] D. Ebert, R. N. Faustov and V. O. Galkin, Eur. Phys. J. C **66**, 197 (2010) [arXiv:0910.5612 [hep-ph]].
[27] M. Di Pierro and E. Eichten, Phys. Rev. D **64**, 114004 (2001) [hep-ph/0104208].
[28] T. Matsuki, T. Morii and K. Sudoh, Eur. Phys. J. A **31**, 701 (2007) [hep-ph/0610186].
[29] T. Matsuki and K. Seo, Phys. Rev. D **85**, 014036 (2012) [arXiv:1111.0857 [hep-ph]].
[30] J. Beringer *et al.* [Particle Data Group Collaboration], Phys.

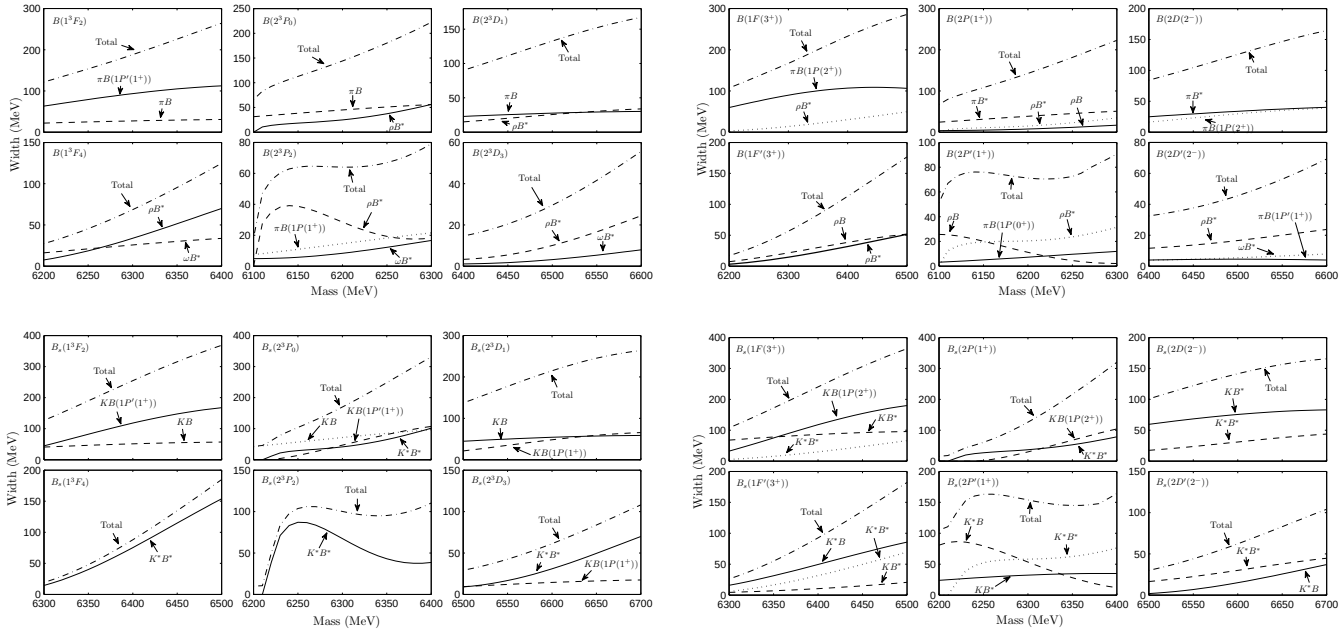

FIG. 12: The variation of the decay widths (in units of MeV) of the higher B and B_s mesons with their masses.

Rev. D **86**, 010001 (2012).

[31] L. Micu, Nucl. Phys. B **10**, 521 (1969).

[32] A. Le Yaouanc, L. Oliver, O. Pene and J. C. Raynal, Phys. Rev. D **8**, 2223 (1973); Phys. Rev. D **9**, 1415 (1974); Phys. Rev. D **11**, 1272 (1975); Phys. Lett. B **72**, 57 (1977); Phys. Lett. B **71**, 397 (1977).

[33] A. Le Yaouanc, L. Oliver, O. Pene and J. C. Raynal, NEW YORK, USA: GORDON AND BREACH (1988) 311p

[34] E. van Beveren, C. Dullemond and G. Rupp, Phys. Rev. D **21**, 772 (1980) [Erratum-ibid. D **22**, 787 (1980)].

[35] E. van Beveren, G. Rupp, T. A. Rijken and C. Dullemond, Phys. Rev. D **27**, 1527 (1983).

[36] R. Bonnaz, B. Silvestre-Brac and C. Gignoux, Eur. Phys. J. A **13**, 363 (2002) [hep-ph/0101112].

[37] W. Roberts, B. Silvestre-Brac, Few Body Syst. **11**, 171 (1992).

[38] B. Zhang, X. Liu, W. -Z. Deng and S. -L. Zhu, Eur. Phys. J. C **50**, 617 (2007) [hep-ph/0609013].

[39] X. Liu, Z. -G. Luo and Z. -F. Sun, Phys. Rev. Lett. **104**, 122001 (2010) [arXiv:0911.3694 [hep-ph]].

[40] Z. -F. Sun, J. -S. Yu, X. Liu and T. Matsuki, Phys. Rev. D **82**, 111501 (2010) [arXiv:1008.3120 [hep-ph]].

[41] Z. -F. Sun and X. Liu, Phys. Rev. D **80**, 074037 (2009) [arXiv:0909.1658 [hep-ph]].

[42] J. -S. Yu, Z. -F. Sun, X. Liu and Q. Zhao, Phys. Rev. D **83**, 114007 (2011) [arXiv:1104.3064 [hep-ph]].

[43] X. Wang, Z. -F. Sun, D. -Y. Chen, X. Liu and T. Matsuki, Phys. Rev. D **85**, 074024 (2012) [arXiv:1202.4139 [hep-ph]].

[44] Z. -C. Ye, X. Wang, X. Liu and Q. Zhao, Phys. Rev. D **86**, 054025 (2012) [arXiv:1206.0097 [hep-ph]].

[45] L. -P. He, X. Wang and X. Liu, Phys. Rev. D **88**, 034008 (2013) [arXiv:1306.5562 [hep-ph]].

[46] H. G. Blundell, hep-ph/9608473.

[47] C. Hayne and N. Isgur, Phys. Rev. D **25**, 1944 (1982).

[48] M. Jacob and G. C. Wick, Annals Phys. **7**, 404 (1959) [Annals Phys. **281**, 774 (2000)].

[49] F. E. Close and E. S. Swanson, Phys. Rev. D **72**, 094004 (2005) [hep-ph/0505206].